Magnetotail Reconnection Asymmetries in a Small, Earth-Like Magnetosphere

Christopher Bard[1] and John C. Dorelli[2]

[1]NASA Goddard Space Flight Center
[2]NASA-GSFC

November 21, 2022

Abstract

We use a newly developed global Hall MHD code to investigate how reconnection drives magnetotail asymmetries in small magnetospheres. Here, we consider a scaled-down, Earth-like magnetosphere where we have artificially inflated the ion inertial length (δ_i) to one Earth radius (the real Earth's $\delta_i\approx 1/15-1/20 R_E \approx 300-400\unit{km}$ in the magnetotail). This results in a magnetotail width on the order of $30 \delta_i$, slightly smaller than Mercury's tail and much smaller than Earth's. At this small size, we find that the Hall effect has significant impact on the global flow pattern, changing from a symmetric, Dungey-like convection under resistive MHD to an asymmetric pattern similar to that found in previous Hall MHD simulations of Ganymede's subsonic magnetosphere as well as other simulations of Mercury's using multi-fluid or embedded kinetic physics. We demonstrate that the Hall effect is sufficient to induce a dawnward asymmetry in observed dipolarization front locations and find quasi-periodic global scale dipolarizations under steady, southward solar wind conditions. On average, we find a thinner current sheet dawnward; however, the measured thickness oscillates with the dipolarization cycle. During the flux-pileup stage, the dawnward current sheet can be thicker than the duskward sheet. This could be an explanation for recent observations that suggest Mercury's current sheet is actually thicker on the duskside: a sampling bias due to a longer-lasting "thick' state in the sheet.

Magnetotail Reconnection Asymmetries in a Small, Earth-Like Magnetosphere

C. Bard[1,2], J. Dorelli[1]

[1]NASA Goddard Space Flight Center
[2]Goddard Planetary Heliophysics Institute, UMBC

Corresponding author: Chris Bard, `christopher.bard@nasa.gov`

Abstract

We use a newly developed global Hall MHD code to investigate how reconnection drives magnetotail asymmetries in small magnetospheres. Here, we consider a scaled-down, Earth-like magnetosphere where we have artificially inflated the ion inertial length (δ_i) to one Earth radius (the real Earth's $\delta_i \approx 1/15 - 1/20\ R_E \approx 300 - 400$ km in the magnetotail). This results in a magnetotail width on the order of 30 δ_i, slightly smaller than Mercury's tail and much smaller than Earth's. At this small size, we find that the Hall effect has significant impact on the global flow pattern, changing from a symmetric, Dungey-like convection under resistive MHD to an asymmetric pattern similar to that found in previous Hall MHD simulations of Ganymede's subsonic magnetosphere as well as other simulations of Mercury's using multi-fluid or embedded kinetic physics. We demonstrate that the Hall effect is sufficient to induce a dawnward asymmetry in observed dipolarization front locations and find quasi-periodic global scale dipolarizations under steady, southward solar wind conditions. On average, we find a thinner current sheet dawnward; however, the measured thickness oscillates with the dipolarization cycle. During the flux-pileup stage, the dawnward current sheet can be thicker than the duskward sheet. This could be an explanation for recent observations that suggest Mercury's current sheet is actually thicker on the duskside: a sampling bias due to a longer-lasting "thick" state in the sheet.

1 Introduction

In planetary magnetospheres, such as Mercury and Earth, observations of plasmoids, flux bundles, and dipolarization fronts (DFs) demonstrate a marked asymmetry in their distribution across the magnetotail. Strangely, these asymmetries are on opposite sides of the tail for different-sized magnetospheres: DFs are mostly found on the dawnside at Mercury (Sun et al., 2016; Dewey et al., 2018), but are found mostly duskward at Earth (Slavin et al., 2005; J. Liu et al., 2013). The existence of asymmetry is thought to arise from physics on scales at or below the ion-inertial length. However, it is debated whether Hall electric fields are sufficient to reproduce this or if other ion/electron scale scale physics are required. Although some authors argue that electron-scale physics is required (Chen et al., 2019), we show in this paper that Hall effects are sufficient to cause an asymmetry in some observed features. Furthermore, it is unknown exactly why Mercury and Earth observe different asymmetries; it is hypothesized that system size effects (relative to the ion inertial length δ_i) play a key role (Lu et al., 2016, 2018; Y.-H. Liu et al., 2019).

In this paper, we investigate of the role of the Hall effect in inducing magnetospheric effects, specifically asymmetry in the magnetotail. Unfortunately, simulating large magnetospheres such as Earth (few hundred δ_i) while properly resolving the small-scale Hall physics requires grid sizes in the billions of cells. Several strategies have been proposed to evade this constraint; one is to embed regions of detailed kinetic physics within large-scale ideal MHD simulations (Chen et al., 2019). This allows for reproduction of kinetic effects within certain regions of the magnetosphere without having to run an expensive, fully kinetic simulation. However, these simulations assume no kinetic effects outside the embedded regions, which are limited to certain regions in the dayside and/or the tail.

Another strategy suggests that we need only set the Hall scale to some length sufficient to capture the essential physics of Hall reconnection without having to fully resolve the physical length scale. In these simulations, the Hall length is set to $\approx 3\%$ of the global scale length (Tóth et al., 2017) which is sufficient to capture the out-of-plane flows and the quadrupolar magnetic field structure induced by the Hall effect. However, recent research in 2D island coalescence (C. Bard & Dorelli, 2018) suggests that although including the Hall term in MHD simulations is sufficient in itself to generate these signatures of Hall reconnection, the actual reconnection rate depends on resolution and numerical resistivity. Although the Hall term is present, the reconnection itself may be Sweet-

Parker-like and slow (unlike fast Hall reconnection). C. Bard and Dorelli (2018) observed that 20-25 cells per δ_i was necessary (within the context of their numerical viscosity) in order to observe fast Hall reconnection. This is much greater than the $5-10$ cells per ion inertial length typically used in simulations (Dorelli et al., 2015; Dong et al., 2019; Chen et al., 2019). This suggests that, although artificially inflating δ_i allows the Hall effect to emerge and have a global impact, much higher resolution is required to observe the universally fast ($\sim 0.1\ v_A$) reconnection observed in kinetic simulations. Finally, C. Bard and Dorelli (2018) found qualitatively different behavior for varying ratios of system size to δ_i: large systems can produce bursty reconnection (with a low average reconnection rate) even when δ_i is sufficiently resolved to produce "fast", instantaneous reconnection. Ultimately, these effects mean that much higher resolution than is currently attainable will be needed to properly model global systems.

These models will require enormous computing power. Fortunately, over the last decade, graphics processing units (GPUs) have proven to be a robust and viable basis for scientific computing. Indeed, several groups have already utilized GPUs to accelerate plasma simulations throughout heliophysics, astrophsyics, and plasma physics (C. M. Bard & Dorelli, 2014; Benítez-Llambay & Masset, 2016; Fatemi et al., 2017; C. Bard & Dorelli, 2018; Schive et al., 2018; Grete et al., 2019; Liska et al., 2019; Y. Wang et al., 2019).

In this paper, we present a magnetosphere simulation code which accelerates the explicit MHD solver algorithm via GPUs. We simulate a "mini-Earth": a magnetosphere with the physical dimensions of Earth's but with the ion inertial length inflated from a few hundred kilometers to 1 R_E and present results on tail asymmetries induced by Hall MHD reconnection. We view this work as a first step in the study of the system-size dependence of magnetic reconnection in Earth-like magnetospheres. We also plan to investigate the role of dipole field strength on magnetosphere reconnection; this will include simulations of Mercury and comparison with MESSENGER data.

This paper is presented as follows: Section 2 provides a brief overview of the Hall MHD algorithm as implemented using GPUs; Section 3 provides the initial condition and setup of the simulation; Section 4 presents tail asymmetries in the simulation and discusses them in the context of observations and proposed theoretical explanations.

2 Methods and Code

We take a Hall MHD code accelerated by graphics processing units using the MPI and NVIDIA CUDA libraries (C. M. Bard & Dorelli, 2014; C. Bard, 2016; C. Bard & Dorelli, 2018) and adapt it to simulate planetary magnetospheres. We review the underlying mathematical equations and algorithms in this section.

Following Powell, Roe, Linde, Gombosi, and De Zeeuw (1999), we split the magnetic field vector $\mathbf{B}$ into a background component $\mathbf{B}_g$ and a perturbed, evolving component $\mathbf{B}_1$ such that $\mathbf{B} = \mathbf{B}_1 + \mathbf{B}_g$. The embedded $\mathbf{B}_g$ is assumed to be static ($\partial \mathbf{B}_g / \partial t = 0$), divergence-free ($\nabla \cdot \mathbf{B}_g = 0$), and curl-free ($\nabla \times \mathbf{B}_g = 0$). In order to preserve the divergence-free constraint on the evolved magnetic field, we solve the "Generalized Lagrangian Multiplier" (GLM) formulation of MHD (Dedner et al., 2002), with additional Hall and electron pressure terms added via Ohm's Law.

The ideal MHD Ohm's law is extended with Hall and isotropic electron pressure terms such that the electric field $\mathbf{E}$ is given by

$$\mathbf{E} = -\frac{\mathbf{v} \times \mathbf{B}}{c} - \frac{\mathbf{J} \times \mathbf{B}}{nec} - \frac{\nabla P_e}{ne} , \tag{1}$$

with c the speed of light, e the electron charge, n the plasma number density, $\mathbf{v}$ the plasma bulk velocity vector, and $\mathbf{J} = \frac{c}{4\pi} \nabla \times \mathbf{B}$ the current density vector. At the moment, we treat the electron pressure P_e as a scalar and assume that it behaves identically to the ion pressure P_i such that $P_e = fP_i$, f being some preselected value of order 0.1. This allows us to write the electron pressure gradient in terms of the total plasma pressure $P = P_e + P_i$: $\nabla P_e = \frac{f}{1+f}\nabla P$. We note that the simulations presented in this paper do not use electron pressure (i.e. $f = 0$).

We normalize the density (ρ), magnetic field, and length scale to reference values ρ_0, B_0, and L_0, respectively. $\mathbf{v}$ is normalized to $v_0 = v_A = B_0/\sqrt{4\pi\rho_0}$, the pressure P to $P_0 = B_0^2/(4\pi)$, and the time t to $t_0 = L_0/v_0$. This results in the set of equations:

$$\frac{\partial \rho}{\partial t} + \nabla \cdot (\rho \mathbf{v}) = 0, \tag{2}$$

$$\frac{\partial \rho \mathbf{v}}{\partial t} + \nabla \cdot \left[\rho \mathbf{v}\mathbf{v} + (p + \frac{B_1^2}{2} + \mathbf{B}_g \cdot \mathbf{B}_1)\mathbb{I} - \mathbf{B}_1\mathbf{B}_1 - \mathbf{B}_g\mathbf{B}_1 - \mathbf{B}_1\mathbf{B}_g\right] = 0, \tag{3}$$

$$\frac{\partial \mathcal{E}}{\partial t} + \nabla \cdot \left[(\frac{\rho v^2}{2} + \frac{\gamma}{\gamma - 1}p)\mathbf{v} + B_1^2\mathbf{v}_T + (\mathbf{B}_g \cdot \mathbf{B}_1)\mathbf{v}_T - (\mathbf{v}_T \cdot \mathbf{B}_1)(\mathbf{B}_g + \mathbf{B}_1) - \frac{\bar{\delta}_i f}{1+f}(\frac{\nabla P}{\rho} \times \mathbf{B}_1)\right] = 0, \tag{4}$$

$$\frac{\partial \mathbf{B}_1}{\partial t} + \nabla \cdot [\mathbf{v}_T\mathbf{B} - \mathbf{B}\mathbf{v}_T] - \frac{\bar{\delta}_i f}{1+f}\nabla \times \frac{\nabla P}{\rho} + \nabla\psi = 0, \tag{5}$$

$$\frac{\partial \psi}{\partial t} + c_h^2 \nabla \cdot \mathbf{B} = -\frac{c_h^2}{c_p^2}\psi, \tag{6}$$

where $\mathcal{E} = \rho v^2/2 + p/(\gamma - 1) + B_1^2/2$ is the total energy density, γ is the ratio of specific heats (taken to be 5/3 in all of our simulations), and $\mathbf{v}_T = \mathbf{v} + \mathbf{v}_H$ combines the bulk velocity ($\mathbf{v}$) with the normalized Hall velocity $\mathbf{v}_H = -\bar{\delta}_i\mathbf{J}/\rho$. The ion inertial length $\delta_i = c\sqrt{m_i}/\sqrt{4\pi n_0 e^2}$ is normalized to the reference length such that $\bar{\delta}_i = \delta_i/L_0$ and set as a fixed parameter. We evaluate the normalized current density ($\mathbf{J} = \nabla \times \mathbf{B_1}$) and the pressure gradient ∇P at cell centers and linearly interpolate to the cell edges when needed. The resulting form is nearly identical to the second-order algorithm with averaging and central differences used to calculate $\mathbf{J}$ in Tóth, Ma, and Gombosi (2008).

ψ is a scalar function whose evolution is designed to be equivalent to $\nabla \cdot \mathbf{B}$; c_h and c_p are parameters for the propagation and dissipation of local $\mathbf{B}$ divergence errors, respectively. Following Dedner et al. (2002), we set c_h as the global maximum wave speed over the individual cells and set c_p such that c_p^2/c_h is within the range $0.05 - 0.5$. Although Dedner et al. (2002) recommended $c_p^2/c_h = 0.18$ and this value works very well to control the magnetic divergence in non-magnetospheric simulations, we find that some level of tweaking is required because of the accumulation of divergence errors at the inner boundary. To ameliorate complications caused by this issue, we separate the momentum equation into a non-magnetic flux and a magnetic source term:

$$\frac{\partial \rho \mathbf{v}}{\partial t} + \nabla \cdot [\rho \mathbf{v}\mathbf{v} + p\mathbb{I}] = \mathbf{J} \times (\mathbf{B_1} + \mathbf{B_g}) \ , \tag{7}$$

which prevents divergence errors from inducing a non-physical acceleration along magnetic field lines (Brackbill & Barnes, 1980), but with some loss of accuracy in evaluating the momentum evolution.

We note that constrained transport methods (e.g. Evans and Hawley (1988); Balsara and Spicer (1999); Dai and Woodward (1998); Londrillo and del Zanna (2004); Stone, Gardiner, Teuben, Hawley, and Simon (2008); Lee and Deane (2009)) are a way to evaluate the magnetic field such that divergence is enforced to machine precision. However, we have found the divergence cleaning+source term method simpler to implement, especially with regards to the magnetosphere-planetary boundary interface.

The overall system is evolved via a time-explicit second-order Runge-Kutta scheme coupled with a simple HLL Riemann solver (Harten et al., 1983; Toro, 1999) and a monotonized central limiter (e.g. Tóth et al. (2008)) with $\beta = 1.25$.

3 Problem Initialization

For our mini-Earth, we chose solar wind and terrestrial magnetic field parameters such that the physical size (in Earth radii) matches that of Earth's magnetosphere and the solar wind ion inertial length evaluates to one Earth radius. In practice, due to normalization, this is functionally equivalent to setting parameters to approximately match the physical conditions of Earth's magnetosphere and simply setting $\delta_i = R_E$ such that $\bar{\delta}_i = R_E/L_0 = 1$. Thus, we set our reference values $L_0 = R_E = 6371\,\mathrm{km}$, $n_0 = 5\,\mathrm{cc}$, $\rho_0 = \mu_H n_0$ (μ_H the mean molecular weight for hydrogen), and $B_0 = 1{\times}10^{-4}\,\mathrm{G}$. From these values, we obtain the other normalization parameters: $v_0 = 97.9{\times}10^5\,\mathrm{cm/s}$, $t_0 \approx 65\,\mathrm{s}$, and $P_0 = 7.96 \times 10^{-10}\,\mathrm{Ba} = 0.0796\,\mathrm{nPa}$.

The solar wind was initialized with values $\rho_{sw} = 1\ \rho_0$, $v_{sw} = 400\,\mathrm{km/s} \approx 4.09\ v_0$, and the wind plasma $\beta_{sw} = 0.305$ such that $P_{sw} = 0.1526\ P_0$. The wind magnetic field is initially set to $\mathbf{B}_{sw} = (-0.174, 0, 0.985)$ for a northward IMF with magnitude $B_{sw} = B_0$. The planetary background magnetic field (B_g) is approximated with dipole moment $(M_x, M_y, M_z) = (0, 0, -0.3\,\mathrm{G})$, and no tilt.

We tried various prescriptions for the inner boundary, including floating (zero-gradient) and fixing various combinations of different variables. Ultimately, although the following inner boundary conditions are not entirely realistic, they allow a stable evolution of the magnetosphere in both the dayside and the tail. We set the inner boundary at a radius of 3 R_E; in these ghost cells, we fix the density at 4 ρ_0, float the pressure, float the radial magnetic field, set the tangential $\mathbf{B}$ to zero, and set the velocity to zero. For the divergence cleaning, we find that simply setting the ghost $\psi_c = 0$ works better than having a floating condition.

For the outer boundaries, the left edge of the simulation domain fixes the conservative variables to the background solar wind condition; the rest of the box has zero-derivative boundaries for all variables.

The simulation coordinates are defined with $-X$ pointing towards the Sun, Z along the planetary magnetic dipole axis, and $+Y$ towards the dusk completing the orthogonal set. In order to resolve the artificially inflated ion inertial length, we choose 5 cells per $\bar{\delta}_i$, giving a minimum resolution of $\Delta x, \Delta y, \Delta z = 0.2L_0$. This resolution is set within the range $-20\ L_0 < x < 20\ L_0; -15\ L_0 < y, z < 15\ L_0$; beyond this the cell length increases by 7% with each additional cell up to a maximum of $5R_E$ or until it hits the boundary. The total size of the grid is $290 \times 253 \times 253$, or just over 18 million cells.

Typically, 10 cells is used to resolve δ_i. However, previous results with island coalescence (C. Bard & Dorelli, 2018) suggest that 5 cell resolution is sufficient for our code to obtain signatures of Hall reconnection, namely the quadrupolar magnetic field structure and the related out-of-plane reconnection outflow. In either case, however, the reconnection is still slow and Sweet-Parker-like; C. Bard and Dorelli (2018) suggest that 20-25 cells/δ_i is required to recover the fast Hall reconnection found by, e.g. Shay, Drake, Rogers, and Denton (2001). Thus, the difference between 5 and 10 cells/δ_i is not significant enough to run the higher-resolution, more computationally expensive simulation, especially for our goal of assessing the global impact of Hall physics on the magnetosphere. We do note that, because $\delta_i \propto 1/\sqrt{\rho}$, a higher resolution does provide more of a buffer against the variability of local δ_i due to density fluctuations.

We start the simulation in ideal MHD ($\bar{\delta}_i = 0$) with a northward IMF ($\mathbf{B}_{sw}$ given above) for 120 t_0, and then flip $B_{z,sw}$ for the southward IMF case and run it for another 120 t_0. At this point, we turn on the Hall term by setting $\bar{\delta}_i = 1$ and run it for another 12 t_0 in order to allow the perturbations induced from the abrupt change of physics to settle. From this point on, the simulation was run for 45 t_0 (representing 48.75 minutes real time) under continuous pure southward IMF and with the Hall term on.

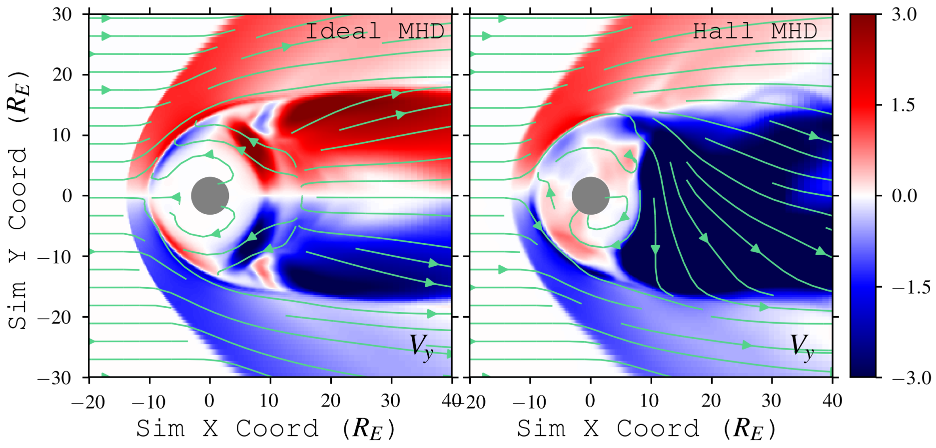

Figure 1: Cross-tail velocity V_y in the tail plane perpendicular to reconnection for both ideal (left) and Hall (right) MHD, normalized to $v_0 = 97.9\,\mathrm{km/s}$. Streamlines show in-plane velocity. A typical Dungey-like, symmetric convection pattern induced by numerical resistivity is clearly demonstrated in ideal MHD. Adding the Hall term induces out-of-reconnection-plane flows which drives an asymmetric convection pattern; this is similar to what has been simulated for Ganymede (Dorelli et al., 2015; Tóth et al., 2016; L. Wang et al., 2018).

4 Results and Discussion

At Earth, a number of studies have found duskward biases in several magnetic phenomena: flux rope occurrence (Slavin et al., 2005; Imber et al., 2011), dipolarization fronts (J. Liu et al., 2013), energetic particle injections (Gabrielse et al., 2014), and reconnection (e.g. Asano et al. (2004); Genestreti, Fuselier, Goldstein, Nagai, and Eastwood (2014)). Additionally, the current sheet was found to be thinner on the duskside (Artemyev et al., 2011; Vasko et al., 2015). Similarly, at Mercury, Poh et al. (2017a) used MESSENGER data to fit the Harris sheet model to 234 tail current sheet crossings and found a bias towards dusk having thinner current sheets (by $\approx 10-30\%$). In contrast, other MESSENGER studies (Sun et al., 2016; Dewey et al., 2018) found dawnward biases in dipolarization events and reconnection front locations. All of these asymmetries are thought to be a result of sub-ion-scale effects (Lu et al., 2018; Y.-H. Liu et al., 2019), though there is still some debate about the exact manifestation and causes of specific asymmetries.

4.1 Hall-induced asymmetry

Prior to turning on the Hall term, the magnetospheric convection is Dungey-type and symmetric about both the $y = 0$ and $z = 0$ planes due to the purely southward magnetic field. Turning the Hall term on, however, induces an out-of-reconnection-plane electric field which breaks that symmetry and drives convection in a preferred direction (Figure 1). For smaller magnetospheres, this effect was first seen in non-ideal MHD simulations of Ganymede (Dorelli et al., 2015; Tóth et al., 2016; L. Wang et al., 2018); this was later seen in 10-moment and embedded-kinetic simulations of Mercury (Dong et al., 2019; Chen et al., 2019). Our simulation supports the idea that it is this Hall-induced drift which produces asymmetries; no kinetic effects are required.

Several studies have proposed mechanisms to explain how Hall reconnection induces asymmetry in the magnetotail. Lu et al. (2016, 2018) (hereafter: Lu+), in studying Earth's magnetotail with global hybrid simulations and localized PIC simulations, showed that the decoupling of ions and electrons within the current sheet (the Hall effect; e.g. Sonnerup (1979)) creates a electric field and associated tail current density. The resulting $\mathbf{E}\times\mathbf{B}$ drift is sufficient to create tail asymmetries and indeed may be the primary cause. The duskside magnetic flux is preferentially evacuated via electron transport dawnward, which leads to a smaller normal B_z and thinner current sheet on the duskside.

In a similar study, Y.-H. Liu et al. (2019) (hereafter: Liu+), using local PIC simulations of embedded, thin current sheets, confirmed that the Hall effect creates electron $\mathbf{E}\times\mathbf{B}$ and diamagnetic drifts which transport magnetic flux dawnward within the current sheet. However, they found that, although the pre-existing tail B_z initially suppresses the onset of dawnside reconnection, the reconnection B_z drives outflows towards dawn and thins out the current sheet on that side. This creates an "active region" of reconnection on the dawn side, which has a thinner current sheet and stronger tail current j_y. After analyzing both these studies, Liu+ proposed that, although the Lu+ model provides a explanation for a duskward bias in the *initial* reconnection onset, the Liu+"active region" provides an explanation for dawnward biases within local, in-progress magnetotail reconnection.

The differences in asymmetry bias within Earth's and Mercury's magnetotails can therefore be explained by system size effects. In small magnetospheres ($\lesssim 50\delta_i$), the "local" current sheet is actually large enough such that the local "dawnside" is physically located on the actual dawn side of the magnetotail. In larger magnetospheres (e.g. with system sizes $\approx 200{-}400\delta_i$), the current sheet lies (mostly) within the dusk side, so its "local dawn" is still within global dusk (or close to the meridian). Thus, these magnetospheres have a duskward bias in current sheet thinness and flux pileup/DFs. We can test several aspects of this general picture within our small magnetosphere.

4.2 Dipolarizations

In our simulation, the Hall electric field induced by tail reconnection accelerates ions towards the duskside and the electrons towards dawn. Since $\delta_i = R_E$ here, the reconnection current sheet spans a significant fraction across the tail; this means that the ions are decoupled from the magnetic field during much of their in-plane convection duskward (blue arrows in Figure 2. The electrons, being coupled to the magnetic field, carry the reconnected, normal B_z flux dawnward (yellow arrows). Because the reconnected magnetic flux originates over a large region within the tail, there is a significant pileup leading to a reconnecting, active region of plasmoid formation on the dawnside. This pileup+reconnection mechanism may be a general cause of dipolarizations in small magnetospheres (like Mercury, e.g. Sundberg et al. (2012)).

In the approximately 48.75 minutes of real time in our simulation there were 7 events on the dawnside (none on the duskside) which followed the general substorm pattern of a buildup/loading phase followed by a unloading (or expansion/relaxation) phase (Rostoker et al., 1980). For each event, we observed pileup of the normal B_z magnetic flux over a period of several minutes, followed by a burst of reconnection and the subsequent ejection of plasmoids tailward (Fig. 3). Three of the eight events produced large plasmoids (on the order of $10R_E = 10\delta_i$), while the rest resulted in smaller ones ($\leq 5R_E$; $\leq 5\delta_i$). The larger ejecta appeared to build up and release on timescales around 10 minutes, while the smaller events had shorter time scales around 5 minutes. Most events originated at a down-tail distance $\approx\ 13 - 16\ R_E$; after ejection, their resulting plasmoids traveled to about $30R_E$ down-tail over several minutes before dissipating.

At Mercury, the timescale for for loading/unloading of magnetic flux in the magnetotail (akin to substorms at Earth) is about 1-3 minutes (Kepko et al., 2015; DiBraccio, 2015). Our longer timescales (5-10 minutes) are likely a result of using Earth-like

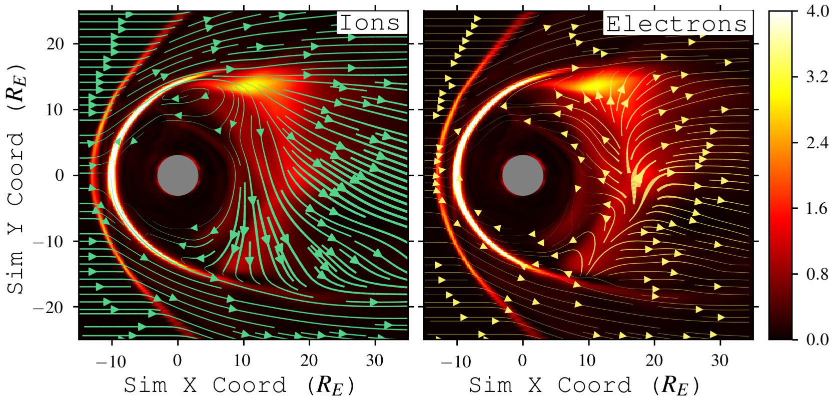

Figure 2: Cross-tail convection in the reconnection plane at $z = 0$, with background color (orange) illustrating relative current sheet density magnitude. Yellow (green) streamlines indicate direction of electron (ion) velocity, with line size proportional to magnitude and normalized relative to the maximum electron (ion) velocity in the plane. The electron velocity (in normalized units) is calculated from $\mathbf{v}_e = \mathbf{v} - \mathbf{J}/\rho$.

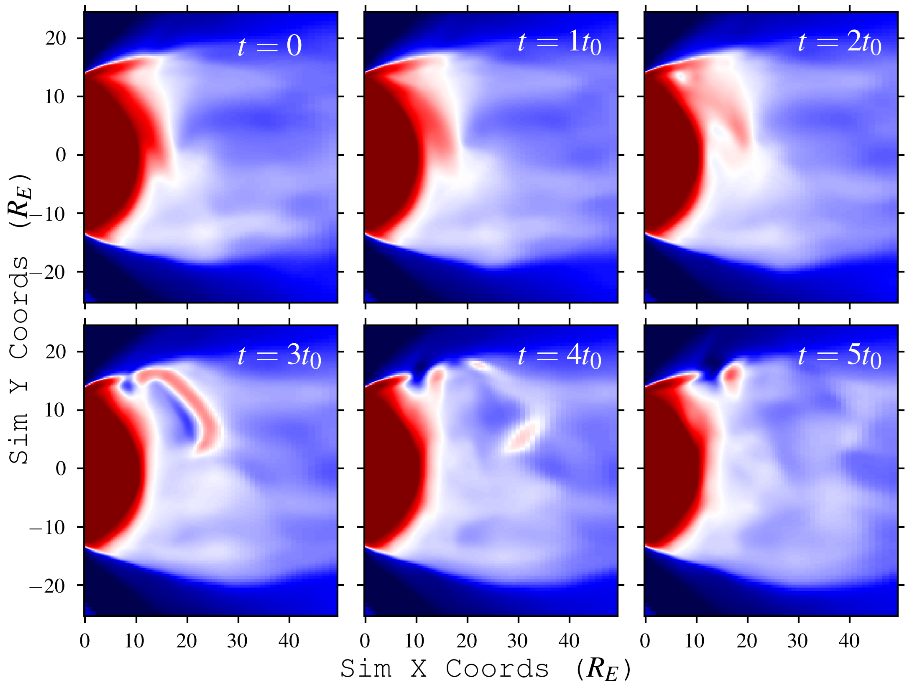

Figure 3: Formation and evolution of a global dipolarization over 5 t_0 $\approx$ 5.4 minutes, as seen in the evolution of magnetotail normal magnetic field B_z (red: out-of-page; blue: into page). Displayed times are relative to upper left image.

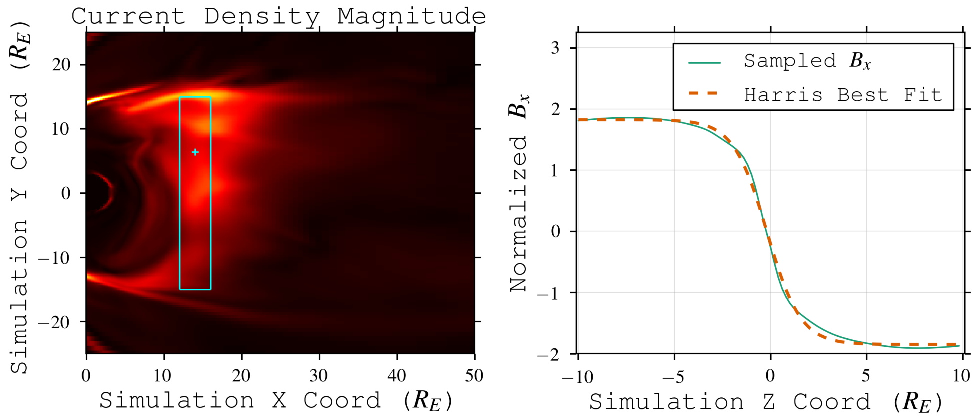

Figure 4: Example of B_x sampling and Harris sheet fit (right figure) as described in text (eq. 8). The left figure shows the magnetotail current sheet magnitude in the simulation $z = 0$ plane; the B_x sampling box domain boundaries are shown in cyan, with the small cross showing the location of the example sample. The box boundaries are $12 < x < 16$ and $-15 < y < 15$.

physical dimensions; our analogue's magnetotail is ≈ 30 planetary radii across while Mercury's is $\approx 5 - 6$.

The observed dawnward bias in dipolarization events for our small magnetosphere corroborates similar dawnward biases found in MESSENGER observations (Sun et al., 2016; Dewey et al., 2018) and global simulations of Mercury (Dong et al., 2019; Chen et al., 2019). It is interesting to note that our results are under a steady, southward solar wind condition; continuous shifts between northward and southward IMF are not required to sustain generation of global substorms. As long as there is Hall-driven convection in the tail, the competition between dawnside B_z pileup and reconnection will drive this cycle. At the moment, it is not clear whether this process is unique to our mini-Earth, since its strong planetary dipole field means that flux piles up over a large swath of the tail. It is possible that a similar process may occur at Mercury, i.e. that its observed dipolarizations are indeed akin to global substorms (Kepko et al., 2015).

We note that, at Earth, there are additional localized (i.e. not global) dipolarization fronts resulting from current sheet instabilities or transient reconnection events (e.g. Runov et al. (2009); Sitnov, Swisdak, and Divin (2009)). We do not see these small-scale fronts in our "mini-Earth"; this may be because we do not have enough down-tail resolution to observe localized current sheet instabilities which form them.

4.3 Current Sheet Thickness

Another test of the Lu+/Liu+ pictures (Section 4.1) is the predicted thickness asymmetry of the tail current sheet. We follow Poh et al. (2017b) and estimate the current sheet thickness in our model by using a Harris sheet (Harris, 1962):

$$B_x = B_0 \tanh \frac{Z - Z_0}{L_{CS}} + \text{offset} \ , \tag{8}$$

where B_0 is the asymptotic lobe field, Z_0 is the current sheet center, L_{CS} is the current sheet half-thickness, and the offset allows for asymmetry between the north and south B_x lobes on either side of the current sheet. We take 6000 one-dimensional cuts of B_x along the north-south direction between $z = \pm 10$ R_E in a volume covering the current

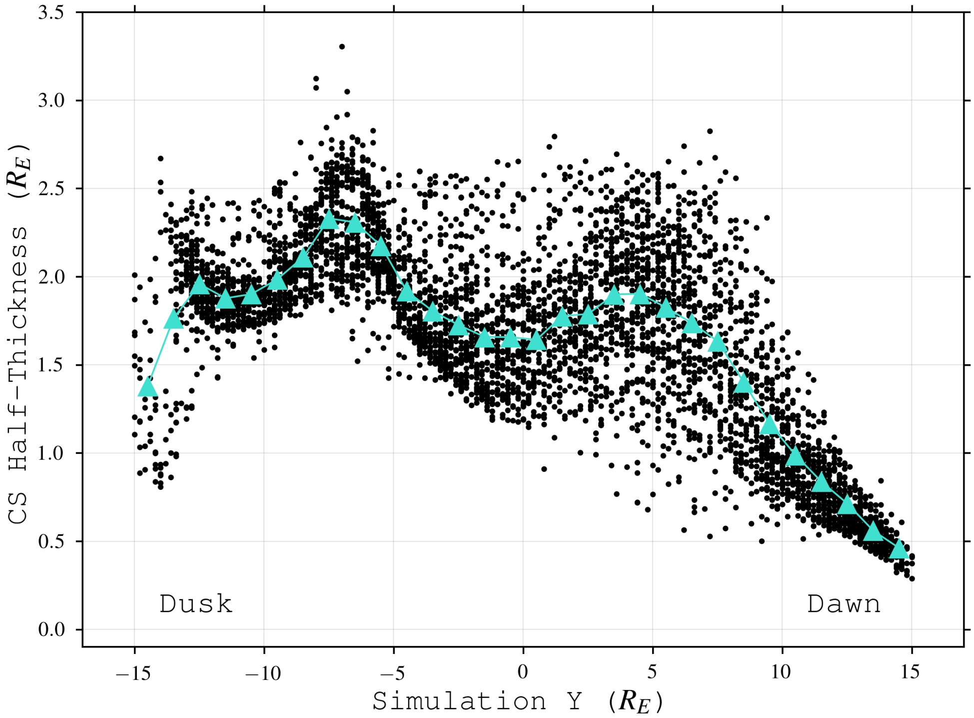

Figure 5: Best-fit current sheet half-thicknesses (L_{CS} derived by fitting eq. 8 to 5037 cuts of B_x along the z-direction. These cuts were randomly sampled in the tail xy-plane and over the simulation time period (see text). There is a bias towards the current sheet being thinner on the dawnside. However, the dawnside also sees a larger spread in thicknesses: this is a result of temporal effects (see main text for discussion).

sheet from $12\ R_E < x < 16\ R_E$ and $-15\ R_E < y < 15\ R_E$, randomly sampled across the box plane and all times (example shown in Fig 4). These cuts are fit to eq. 8 using the Levenberg-Marquadt least-squares algorithm in scipy.curvefit (Virtanen et al., 2020); instances that do not fit well ($\chi^2 > 0.01$) or that return nonsensical results ($L_{CS} < 0$) are rejected. This results in 5037 samples of the current sheet thickness across the magnetotail (Figure 5). This distribution shows that the dawnward current sheet is thinner on average than the duskward sheet. However, there is a significant scatter in this result; the dawn sheet covers a wider range of thicknesses. This variation is caused by the dawnside pileup+reconnection mechanism.

The current sheet oscillates with the dipolarization cycle (Sec. 4.2) between a "thick state" due to the B_z pileup and a "thin state" immediately following the flux unloading and plasmoid ejection. This is demonstrated in Fig. 6, where fitted CS thicknesses during both flux loading and unloading stages are plotted along with snapshots of the B_z state. During the loading stage, the piled-up flux on the dawnside ($5R_E < y < 12R_E$) fattens the current sheet; here, the sampled dawn thicknesses are comparable to and can exceed the dusk thicknesses. However, after the unloading stage, the current sheet on the dawnside is much thinner where the flux has been evacuated (bottom right plot; $R > 15R_E$). Interestingly, we can see that where the B_z flux remains ($R < 15R_E$), the current sheet continues to be thick. Combining all the sample fits over several cycles of loading and unloading results in the picture shown in Fig. 5: a dawnward current sheet moving between thick and thin states depending on the level of flux pileup. Indeed, this is

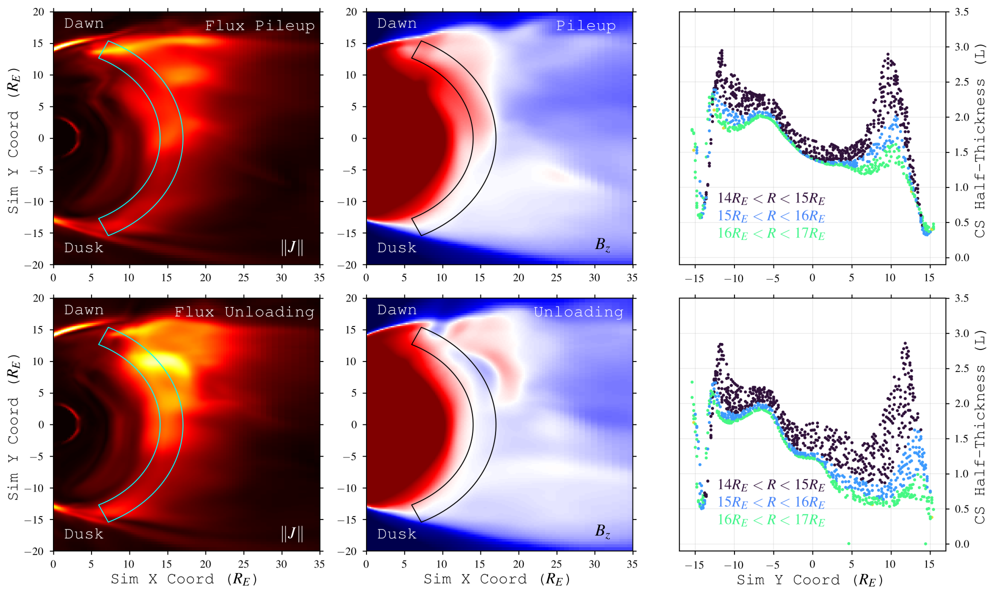

Figure 6: Cross-comparison of current sheet density magnitude (left), current sheet B_z flux pileup (center; same parameters as Fig. 3) and sampled thicknesses (right) during (top row) and after (bottom row) a global dipolarization event. Current sheet fits are sampled from the area within the wedges ($14R_E < R < 17R_E$). The current sheet is thick where the B_z flux has piled up, and thin where the flux has been unloaded.

a common pattern throughout the simulation: where there is flux pileup, the current sheet is thicker and the current density is lower (e.g. Fig. 7).

This cycle may explain the apparent contradiction between the Liu+ prediction of thinner dawnward current sheets in small magnetospheres and the Poh et al. (2017a) spacecraft observation of thicker dawnward sheets at Mercury. Even though, on average, the current sheet is thinner dawnward (as Liu+ predicts), the sampling of measurements could be producing the opposite result. As shown in Figs. 5 and 6, the sampled sheet thickness can greatly depend on where and when the craft crosses the tail. In our simulation, the current sheet is continuously morphing between "thick" and "thin" states; both types of regions exist simultaneously within the dawnside. Most points in the tail preferentially see thicker sheets over time, though some preferentially see thinner sheets. It is possible that these effects combine to produce a sampling bias in time and space towards thicker sheets. This will need more investigation, especially with regard to the varying solar wind conditions and seasons that MESSENGER experiences at Mercury.

5 Conclusion

We have simulated a small, "mini-Earth" in which which the physical dimensions are like Earth's, but with the ion-scale length δ_i artificially inflated to 1 R_E. We find that Hall effects are sufficient to generate tail asymmetries in dipolarization, plasmoids, and current sheet thickness; no electron-scale physics are required, though they may contribute to these or other asymmetries. Furthermore, we note that the observed asymmetries in our simulation do not appear in the ideal MHD portion of our run. Thus, we conclude that adding Hall physics is sufficient to generate asymmetry in the tail (in contrast with Chen et al. (2019), who argue that electron-scale effects are required). However, some questions still remain concerning observed asymmetries at Earth and Mercury and dif-

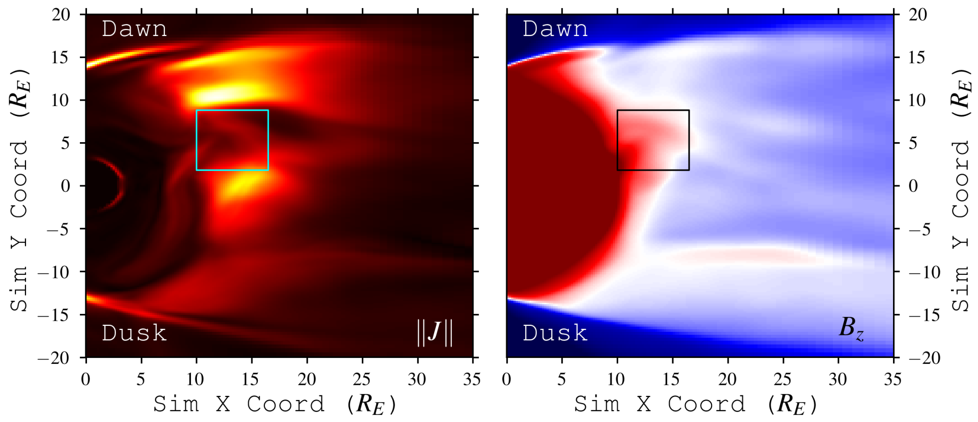

Figure 7: Cross-comparison of current density magnitude $\|J\|$ and normal magnetic field B_z in the tail plane at a selected snapshot time. The local pileup of magnetic flux thickens the current sheet, resulting in a lower current density and impeding local reconnection.

ferences between tail asymmetries across system sizes. It is possible that including kinetic effects may better reproduce specific observed asymmetries, though they are not needed for a general explanation of tail asymmetry.

In general, our simulation appears to corroborate the Liu+ picture of tail asymmetry in small magnetospheres; however, the Lu+ finding that the transported tail B_z thickens the current sheet is readily manifested here. Although the reconnected B_z does drive outflows and thin current sheets on the dawnside, we see that it can pile up and thicken current sheets. There is a continuous cycle between the dawnward transport of B_z leading to pileup (which thickens the current sheet) and reconnection (which thins the current sheet); this manifests in an oscillating current sheet thickness. On average, we find the current sheet is thinner on the dawnside, but it can occasionally be thicker in some regions depending on the level of flux pileup.

Further study will be required to confirm or contrast this picture for larger magnetospheres. Since our simulation is of a “mini-Earth” magnetosphere, several questions concerning more realistic magnetotails remain:

- How does the weaker, offset dipole of Mercury affect the amount of magnetic flux available for transport/pileup and the resulting plasmoid formation/ejection?
- Are the observed dipolarizations at Mercury actually “global”, like substorms?
- How does increasing the system size/δ_i ratio affect tail convection, transport of B_z, and plasmoid/DF formation?
- What other effects (e.g. kinetic, ionosphere) cause asymmetries and how do they interact with one another?

We look forward to future studies which will investigate these questions in greater detail.

Acknowledgments

The authors acknowledge funding from NASAs Heliophysics Internal Scientist Funding Model (HISFM) program. C.B.’s software development was partly supported by an appointment to the NASA Postdoctoral Program at NASA-Goddard Space Flight Center, administered by Universities Space Research Association under contract with NASA. C.B. thanks Alex Glocer for useful discussions concerning simulation techniques. C.B. thanks Ryan Dewey for helpful discussions concerning Mercury tail asymmetries/MESSENGER observations. Observational data was not used, nor created for this research; the model algorithm and simulation parameters are described in detail above.

References

Artemyev, A. V., Petrukovich, A. A., Nakamura, R., & Zelenyi, L. M. (2011, September). Cluster statistics of thin current sheets in the Earth magnetotail: Specifics of the dawn flank, proton temperature profiles and electrostatic effects. *Journal of Geophysical Research (Space Physics)*, *116*(A9), A09233. doi: 10.1029/2011JA016801

Asano, Y., Mukai, T., Hoshino, M., Saito, Y., Hayakawa, H., & Nagai, T. (2004, February). Current sheet structure around the near-Earth neutral line observed by Geotail. *Journal of Geophysical Research (Space Physics)*, *109*(A2), A02212. doi: 10.1029/2003JA010114

Balsara, D. S., & Spicer, D. S. (1999, March). A Staggered Mesh Algorithm Using High Order Godunov Fluxes to Ensure Solenoidal Magnetic Fields in Magnetohydrodynamic Simulations. *Journal of Computational Physics*, *149*, 270-292. doi: 10.1006/jcph.1998.6153

Bard, C. (2016). *Tools for Studying Magnetospheric-Wind Interactions* (Unpublished doctoral dissertation). The University of Wisconsin - Madison.

Bard, C., & Dorelli, J. C. (2018, February). On the role of system size in Hall MHD magnetic reconnection. *Physics of Plasmas*, *25*(2), 022103. doi: 10.1063/1.5010785

Bard, C. M., & Dorelli, J. C. (2014, February). A simple GPU-accelerated two-dimensional MUSCL-Hancock solver for ideal magnetohydrodynamics. *Journal of Computational Physics*, *259*, 444-460. doi: 10.1016/j.jcp.2013.12.006

Benítez-Llambay, P., & Masset, F. S. (2016, March). FARGO3D: A New GPU-oriented MHD Code. , *223*(1), 11. doi: 10.3847/0067-0049/223/1/11

Brackbill, J. U., & Barnes, D. C. (1980, May). The effect of nonzero product of magnetic gradient and B on the numerical solution of the magnetohydrodynamic equations. *Journal of Computational Physics*, *35*, 426-430. doi: 10.1016/0021-9991(80)90079-0

Chen, Y., Tóth, G., Jia, X., Slavin, J. A., Sun, W., Markidis, S., … Raines, J. M. (2019, November). Studying Dawn-Dusk Asymmetries of Mercury's Magnetotail Using MHD-EPIC Simulations. *Journal of Geophysical Research (Space Physics)*, *124*(11), 8954-8973. doi: 10.1029/2019JA026840

Dai, W., & Woodward, P. R. (1998). On the divergence-free condition and conservation laws in numerical simulations for supersonic magnetohydrodynamic flows. *Astrophys. J.*, *494*, 317-355.

Dedner, A., Kemm, F., Kröner, D., Munz, C.-D., Schnitzer, T., & Wesenberg, M. (2002, January). Hyperbolic Divergence Cleaning for the MHD Equations. *Journal of Computational Physics*, *175*, 645-673. doi: 10.1006/jcph.2001.6961

Dewey, R. M., Raines, J. M., Sun, W., Slavin, J. A., & Poh, G. (2018, October). MESSENGER Observations of Fast Plasma Flows in Mercury's Magnetotail. , *45*(19), 10,110-10,118. doi: 10.1029/2018GL079056

DiBraccio, G. A. (2015, April). MESSENGER Observations of Mercury's Magnetosphere Dynamics: A Review (Invited). In *Egu general assembly conference abstracts* (p. 8051).

Dong, C., Wang, L., Hakim, A., Bhattacharjee, A., Slavin, J. A., DiBraccio, G. A., & Germaschewski, K. (2019, November). Global Ten-Moment Multifluid Simulations of the Solar Wind Interaction with Mercury: From the Planetary

Conducting Core to the Dynamic Magnetosphere. , *46*(21), 11,584-11,596. doi: 10.1029/2019GL083180

Dorelli, J. C., Glocer, A., Collinson, G., & Tóth, G. (2015, July). The role of the Hall effect in the global structure and dynamics of planetary magnetospheres: Ganymede as a case study. *Journal of Geophysical Research (Space Physics)*, *120*, 5377-5392. doi: 10.1002/2014JA020951

Evans, C. R., & Hawley, J. F. (1988, September). Simulation of magnetohydrodynamic flows - A constrained transport method. *Astrophys. J.*, *332*, 659-677. doi: 10.1086/166684

Fatemi, S., Poppe, A. R., Delory, G. T., & Farrell, W. M. (2017, May). AMITIS: A 3D GPU-Based Hybrid-PIC Model for Space and Plasma Physics. In *Journal of physics conference series* (Vol. 837, p. 012017). doi: 10.1088/1742-6596/837/1/012017

Gabrielse, C., Angelopoulos, V., Runov, A., & Turner, D. L. (2014, April). Statistical characteristics of particle injections throughout the equatorial magnetotail. *Journal of Geophysical Research (Space Physics)*, *119*(4), 2512-2535. doi: 10.1002/2013JA019638

Genestreti, K. J., Fuselier, S. A., Goldstein, J., Nagai, T., & Eastwood, J. P. (2014, December). The location and rate of occurrence of near-Earth magnetotail reconnection as observed by Cluster and Geotail. *Journal of Atmospheric and Solar-Terrestrial Physics*, *121*, 98-109. doi: 10.1016/j.jastp.2014.10.005

Grete, P., Glines, F. W., & O'Shea, B. W. (2019, May). K-Athena: a performance portable structured grid finite volume magnetohydrodynamics code. *arXiv e-prints*, arXiv:1905.04341.

Harris, E. G. (1962, January). On a plasma sheath separating regions of oppositely directed magnetic field. *Il Nuovo Cimento*, *23*(1), 115-121. doi: 10.1007/BF02733547

Harten, A., Lax, P., & van Leer, B. (1983). On upstream differencing and godunov type methods for hyperbolic conservation laws. *SIAM Review*, *25*, 35-61.

Imber, S. M., Slavin, J. A., Auster, H. U., & Angelopoulos, V. (2011, February). A THEMIS survey of flux ropes and traveling compression regions: Location of the near-Earth reconnection site during solar minimum. *Journal of Geophysical Research (Space Physics)*, *116*(A2), A02201. doi: 10.1029/2010JA016026

Kepko, L., Glassmeier, K. H., Slavin, J. A., & Sundberg, T. (2015, January). Substorm Current Wedge at Earth and Mercury. In *Magnetotails in the solar system* (Vol. 207, p. 361-372). doi: 10.1002/9781118842324.ch21

Lee, D., & Deane, A. E. (2009, March). An unsplit staggered mesh scheme for multidimensional magnetohydrodynamics. *Journal of Computational Physics*, *228*, 952-975. doi: 10.1016/j.jcp.2008.08.026

Liska, M., Chatterjee, K., Tchekhovskoy, A. e., Yoon, D., van Eijnatten, D., Hesp, C., … van der Klis, M. (2019, December). H-AMR: A New GPU-accelerated GRMHD Code for Exascale Computing With 3D Adaptive Mesh Refinement and Local Adaptive Time-stepping. *arXiv e-prints*, arXiv:1912.10192.

Liu, J., Angelopoulos, V., Runov, A., & Zhou, X. Z. (2013, May). On the current sheets surrounding dipolarizing flux bundles in the magnetotail: The case for wedgelets. *Journal of Geophysical Research (Space Physics)*, *118*(5), 2000-2020. doi: 10.1002/jgra.50092

Liu, Y.-H., Li, T. C., Hesse, M., Sun, W. J., Liu, J., Burch, J., … Huang, K. (2019, April). Three-Dimensional Magnetic Reconnection With a Spatially Confined X-Line Extent: Implications for Dipolarizing Flux Bundles and the Dawn-Dusk Asymmetry. *Journal of Geophysical Research (Space Physics)*, *124*(4), 2819-2830. doi: 10.1029/2019JA026539

Londrillo, P., & del Zanna, L. (2004, March). On the divergence-free condition in Godunov-type schemes for ideal magnetohydrodynamics: the upwind constrained transport method. *Journal of Computational Physics*, *195*, 17-48. doi:

10.1016/j.jcp.2003.09.016

Lu, S., Lin, Y., Angelopoulos, V., Artemyev, A. V., Pritchett, P. L., Lu, Q., & Wang, X. Y. (2016, December). Hall effect control of magnetotail dawn-dusk asymmetry: A three-dimensional global hybrid simulation. *Journal of Geophysical Research (Space Physics)*, *121*(12), 11,882-11,895. doi: 10.1002/2016JA023325

Lu, S., Pritchett, P. L., Angelopoulos, V., & Artemyev, A. V. (2018, April). Formation of Dawn-Dusk Asymmetry in Earth's Magnetotail Thin Current Sheet: A Three-Dimensional Particle-In-Cell Simulation. *Journal of Geophysical Research (Space Physics)*, *123*(4), 2801-2814. doi: 10.1002/2017JA025095

Poh, G., Slavin, J. A., Jia, X., Raines, J. M., Imber, S. M., Sun, W.-J., ... Smith, A. W. (2017a, August). Coupling between Mercury and its nightside magnetosphere: Cross-tail current sheet asymmetry and substorm current wedge formation. *Journal of Geophysical Research (Space Physics)*, *122*(8), 8419-8433. doi: 10.1002/2017JA024266

Poh, G., Slavin, J. A., Jia, X., Raines, J. M., Imber, S. M., Sun, W.-J., ... Smith, A. W. (2017b, January). Mercury's cross-tail current sheet: Structure, X-line location and stress balance. , *44*(2), 678-686. doi: 10.1002/2016GL071612

Powell, K. G., Roe, P. L., Linde, T. J., Gombosi, T. I., & De Zeeuw, D. L. (1999, September). A Solution-Adaptive Upwind Scheme for Ideal Magnetohydrodynamics. *Journal of Computational Physics*, *154*, 284-309. doi: 10.1006/jcph.1999.6299

Rostoker, G., Akasofu, S. I., Foster, J., Greenwald, R. A., Kamide, Y., Kawasaki, K., ... Russell, C. T. (1980, April). Magnetospheric substorms-definition and signatures. , *85*(A4), 1663-1668. doi: 10.1029/JA085iA04p01663

Runov, A., Angelopoulos, V., Sitnov, M. I., Sergeev, V. A., Bonnell, J., McFadden, J. P., ... Auster, U. (2009, July). THEMIS observations of an earthward-propagating dipolarization front. , *36*(14), L14106. doi: 10.1029/2009GL038980

Schive, H.-Y., ZuHone, J. A., Goldbaum, N. J., Turk, M. J., Gaspari, M., & Cheng, C.-Y. (2018, December). GAMER-2: a GPU-accelerated adaptive mesh refinement code - accuracy, performance, and scalability. , *481*, 4815-4840. doi: 10.1093/mnras/sty2586

Shay, M. A., Drake, J. F., Rogers, B. N., & Denton, R. E. (2001, March). Alfvénic collisionless magnetic reconnection and the Hall term. , *106*, 3759-3772. doi: 10.1029/1999JA001007

Sitnov, M. I., Swisdak, M., & Divin, A. V. (2009, April). Dipolarization fronts as a signature of transient reconnection in the magnetotail. *Journal of Geophysical Research (Space Physics)*, *114*(A4), A04202. doi: 10.1029/2008JA013980

Slavin, J. A., Tanskanen, E. I., Hesse, M., Owen, C. J., Dunlop, M. W., Imber, S., ... Glassmeier, K. H. (2005, June). Cluster observations of traveling compression regions in the near-tail. *Journal of Geophysical Research (Space Physics)*, *110*(A6), A06207. doi: 10.1029/2004JA010878

Sonnerup, B. U. Ö. (1979). Magnetic field reconnection. In *Solar system plasma physics* (Vol. 3, p. 45-108).

Stone, J. M., Gardiner, T. A., Teuben, P., Hawley, J. F., & Simon, J. B. (2008, September). Athena: A New Code for Astrophysical MHD. *Astrophys. J., Suppl. Ser.*, *178*, 137-177. doi: 10.1086/588755

Sun, W. J., Fu, S. Y., Slavin, J. A., Raines, J. M., Zong, Q. G., Poh, G. K., & Zurbuchen, T. H. (2016, August). Spatial distribution of Mercury's flux ropes and reconnection fronts: MESSENGER observations. *Journal of Geophysical Research (Space Physics)*, *121*(8), 7590-7607. doi: 10.1002/2016JA022787

Sundberg, T., Slavin, J. A., Boardsen, S. A., Anderson, B. J., Korth, H., Ho, G. C., ... Solomon, S. C. (2012, September). MESSENGER observations of dipolarization events in Mercury's magnetotail. *Journal of Geophysical Research*

(Space Physics), *117*, A00M03. doi: 10.1029/2012JA017756

Toro, E. F. (1999). *Riemann solvers and numerical methods for fluid dynamics: A practical introduction.* Springer-Verlag.

Tóth, G., Chen, Y., Gombosi, T. I., Cassak, P., Markidis, S., & Peng, I. B. (2017, October). Scaling the Ion Inertial Length and Its Implications for Modeling Reconnection in Global Simulations. *Journal of Geophysical Research (Space Physics)*, *122*, 10. doi: 10.1002/2017JA024189

Tóth, G., Jia, X., Markidis, S., Peng, I. B., Chen, Y., Daldorff, L. K. S., ... Dorelli, J. C. (2016, February). Extended magnetohydrodynamics with embedded particle-in-cell simulation of Ganymede's magnetosphere. *Journal of Geophysical Research (Space Physics)*, *121*, 1273-1293. doi: 10.1002/2015JA021997

Tóth, G., Ma, Y., & Gombosi, T. I. (2008, July). Hall magnetohydrodynamics on block-adaptive grids. *Journal of Computational Physics*, *227*, 6967-6984. doi: 10.1016/j.jcp.2008.04.010

Vasko, I. Y., Petrukovich, A. A., Artemyev, A. V., Nakamura, R., & Zelenyi, L. M. (2015, October). Earth's distant magnetotail current sheet near and beyond lunar orbit. *Journal of Geophysical Research (Space Physics)*, *120*(10), 8663-8680. doi: 10.1002/2015JA021633

Virtanen, P., Gommers, R., Oliphant, T. E., Haberland, M., Reddy, T., Cournapeau, D., ... Contributors, S. . . (2020). SciPy 1.0: Fundamental Algorithms for Scientific Computing in Python. *Nature Methods*, *17*, 261–272. doi: https://doi.org/10.1038/s41592-019-0686-2

Wang, L., Germaschewski, K., Hakim, A., Dong, C., Raeder, J., & Bhattacharjee, A. (2018, April). Electron Physics in 3-D Two-Fluid 10-Moment Modeling of Ganymede's Magnetosphere. *Journal of Geophysical Research (Space Physics)*, *123*, 2815-2830. doi: 10.1002/2017JA024761

Wang, Y., Feng, X., Zhou, Y., & Gan, X. (2019, May). A multi-GPU finite volume solver for magnetohydrodynamics-based solar wind simulations. *Computer Physics Communications*, *238*, 181-193. doi: 10.1016/j.cpc.2018.12.003